Characteristic Structure and Growth of the Nonprecipitating Cumulus Layer over South Florida

RICHARD H. JOHNSON[1]

National Hurricane and Experimental Meteorology Laboratory, NOAA, Coral Gables, FL 33124

(Manuscript received 17 April 1978, in final form 16 June 1978)

ABSTRACT

A study has been carried out of the structure of the planetary boundary layer over south central Florida under locally undisturbed conditions using data from the 1975 Florida Area Cumulus Experiment (FACE). From a series of rawinsonde observations (129 total) during July and August at approximately 1000, 1300 and 1600 LST, 24 soundings have been identified as revealing both mixed-layer and cumulus-layer structures. The soundings have been composited to provide a representation of the average structure of the two layers. The inversion that is found to exist at the top of the cumulus layer is much less pronounced than the trade wind inversion as might be expected considering the relatively rapid growth and short lifetime of this phenomenon.

A model for the growth of the mixed and cumulus layers is presented that includes effects of updraft mass flux, detrainment and evaporation. A closure assumption is proposed that relates the buoyancy flux in the cloud environment at the base of the cumulus inversion to the buoyancy flux within cumulus updrafts at that level. Application of the model to the 1975 FACE data has provided lower bound estimates to the downward buoyancy flux at the cumulus inversion.

1. Introduction

Characteristics of the trade wind inversion over tropical oceanic regions, its vertical structure and downstream variation, have been well documented for many years (Ficker, 1936; Bunker *et al.*, 1949; Riehl *et al.*, 1951; Malkus, 1958). Observations from more recent experiments, the Atlantic Trade Wind Experiment (ATEX) and the Barbados Oceanographic and Meteorological Experiment (BOMEX) in 1969, have provided a definitive description of the structure of the tropical atmospheric boundary layer during generally undisturbed conditions (e.g., Augstein *et al.*, 1974; Garstang and Betts, 1974). These experiments have defined the following features of the trade wind boundary layer: a shallow surface layer, mixed layer (with nearly constant potential temperature and mixing ratio), transition layer, trade wind cumulus layer and trade wind inversion layer (shown schematically in Fig. 5). Not surprisingly, during undisturbed conditions over tropical continental regions a cumulus layer having a structure similar to that of the trade wind cumulus layer can be frequently observed. Such a structure has in fact been observed during late morning and afternoon hours in the summer months over a subtropical continental region, south central Florida. This paper reports on a series of rawinsonde observations taken during the summer 1975 FACE (Florida Area Cumulus Experiment) that have been used to determine the structure and time evolution of the mixed and cumulus layers over south central Florida.

In contrast to the quasi-stationary nature of the trade wind cumulus layer over tropical oceanic regions during undisturbed conditions, at least in a horizontally averaged sense, the mixed and cumulus layers over land exhibit a significant diurnal variation as a consequence of diurnally varying surface heating. The time evolution of the mixed layer over south Florida and the effects of cumulus convection on its growth have been investigated by Johnson (1977). It was found that under locally undisturbed conditions over the central peninsula rapid growth of the mixed layer commences at about 2 or 3 h after sunrise continuing until shortly before noon at which time a marked reduction in the growth rate occurs. This reduced rate of growth of the mixed layer nearly 2 h before the maximum surface buoyancy flux is attributed to mesoscale (~10–100 km) subsidence that occurs over the peninsula as a result of compensating downward motion in the environment surrounding deep convection. It may well be that the south Florida sea breeze circulation also contributes to the observed subsidence as indicated in the model results of Pielke (1974). It was further found that the maximum environmental sinking occurs several hours

[1] Present affiliation: Atmospheric Sciences, University of Wisconsin, Milwaukee 53201.

0027-0644/78/1495-1504$05.00

before the time of the heaviest peninsula-scale rainfall, indicating that the intensity of cumulus downdrafts relative to updrafts over the peninsula increases as the convective activity increases during the day.

While simple mixed-layer theory (e.g., Carson, 1973; Tennekes, 1973) has proven quite successful in predicting the development of the mixed layer under cloudless conditions, a closed theory for the more complex problem of the growth of the mixed and cumulus layers, one that does not require specification of cloud thermodynamic properties or mass fluxes, cumulus layer lapse rates or other properties of the cumulus layer, has yet to be achieved. Nevertheless, further insight into cumulus layer dynamics and thermodynamics has been realized from a number of studies of nonprecipitating cumulus convection (Lilly, 1968; Betts, 1973, 1976; Mak, 1976; Ogura, 1977; Ogura *et al.*, 1977; Albrecht, 1977). Betts (1976) has proposed a model for the subcloud layer that couples a single cloud mass flux model with a subcloud layer budget to examine several aspects of the time development of a cumulus-topped mixed layer. Mak (1976) and Ogura (1977) examined the horizontal variation in the depth of the trade wind inversion, taking into account the physical processes of cloud liquid water evaporation and downward turbulent heat flux in the trade wind inversion layer. Ogura *et al.* (1977) have proposed a steady-state model for the trade wind inversion that assumes a spectrum of cloud sizes within a cumulus layer having prescribed lapse rates of temperature and mixing ratio. It is assumed that the heat and moisture fluxes at the base of the trade wind inversion are accomplished entirely by cloud updrafts, while descending motion is distributed uniformly throughout the cloud environment. A time-dependent model of the cloud and subcloud layers has recently been developed by Albrecht (1977). He incorporates a cloud model that features cumulus mass flux and cloud-environment temperature and moisture differences varying linearly with height. The model, which also includes radiative effects, appears to rather successfully predict the observed structure of the trade wind inversion.

Although the primary purpose of this paper is to present a documentation of the structure and growth of the mixed and cumulus layers over south central Florida, an attempt to achieve some understanding of growth behavior over this region using a simple coupled model for the two layers is made. A closure assumption is proposed that relates the buoyancy flux in the cloud environment at the base of the cumulus inversion (the overland counterpart of the trade wind inversion) to the buoyancy flux within cumulus updrafts at that level. Owing to the lack of direct measurements of the mean mesoscale vertical motion over the region of study, however, a complete testing of the model cannot be made. The limited number of conclusions that can be drawn based on the model are reported in Section 5.

2. The Experiment

The 1975 Florida Area Cumulus Experiment (FACE) represents the most intensive of a series of summer experiments directed in part toward further understanding of moist convective processes over south central Florida (Simpson and Woodley, 1975). During the 1975 experiment from 16 June to 15 September a dense surface meteorological network was operated just south of Lake Okeechobee. Within a 34 km × 48 km rectangular region a mesoscale network of instruments was established to record wind, pressure, temperature, relative humidity and rainfall. Included in the network was a single rawinsonde tracking station approximately 20 km south of the lake and 100 km inland from both the east and west coastlines. Three rawinsondes per day were released, whenever possible, at 1000, 1300 and 1600 (all times LST) during July and August. The sounding instruments for the entire experiment were a combination of omegasondes and conventional sondes (Johnson, 1977); however, all soundings used in this study were from omegasonde instrumentation.

Although details regarding the data resolution, errors and reduction procedures were given in Johnson (1977), it is important to repeat here some of this information since it bears directly on the results of this study. For example, the ability to adequately define the cumulus inversion (a level marked by increased stability at the top of the cumulus layer) depends critically on the resolution capabilities of the sounding instruments. The omegasondes provided a nearly continuous record of temperature and relative humidity having ~1.5 mb resolution in the lower troposhere. Since the data were extracted manually from strip charts, a method was devised to extract only significant level data, with the levels being selected in such a way that a linear variation between successive values of temperature and relative humidity restricted deviations from observed values in the interval to less than 0.5 K and 5%, respectively. This method provided an effective resolution on the order of 10 mb. A check on the validity of this approach on a subset of 13 soundings that ascended into the base of nonprecipitating cumuli showed that this method reproduced results obtained by extraction at 10 mb intervals very accurately within the subcloud layer (Johnson, 1977). As in the study of Johnson, corrections for the thermal lags of the thermistor and hygrister have not been made. Consequently, as before, estimates of cloud-base height, which are

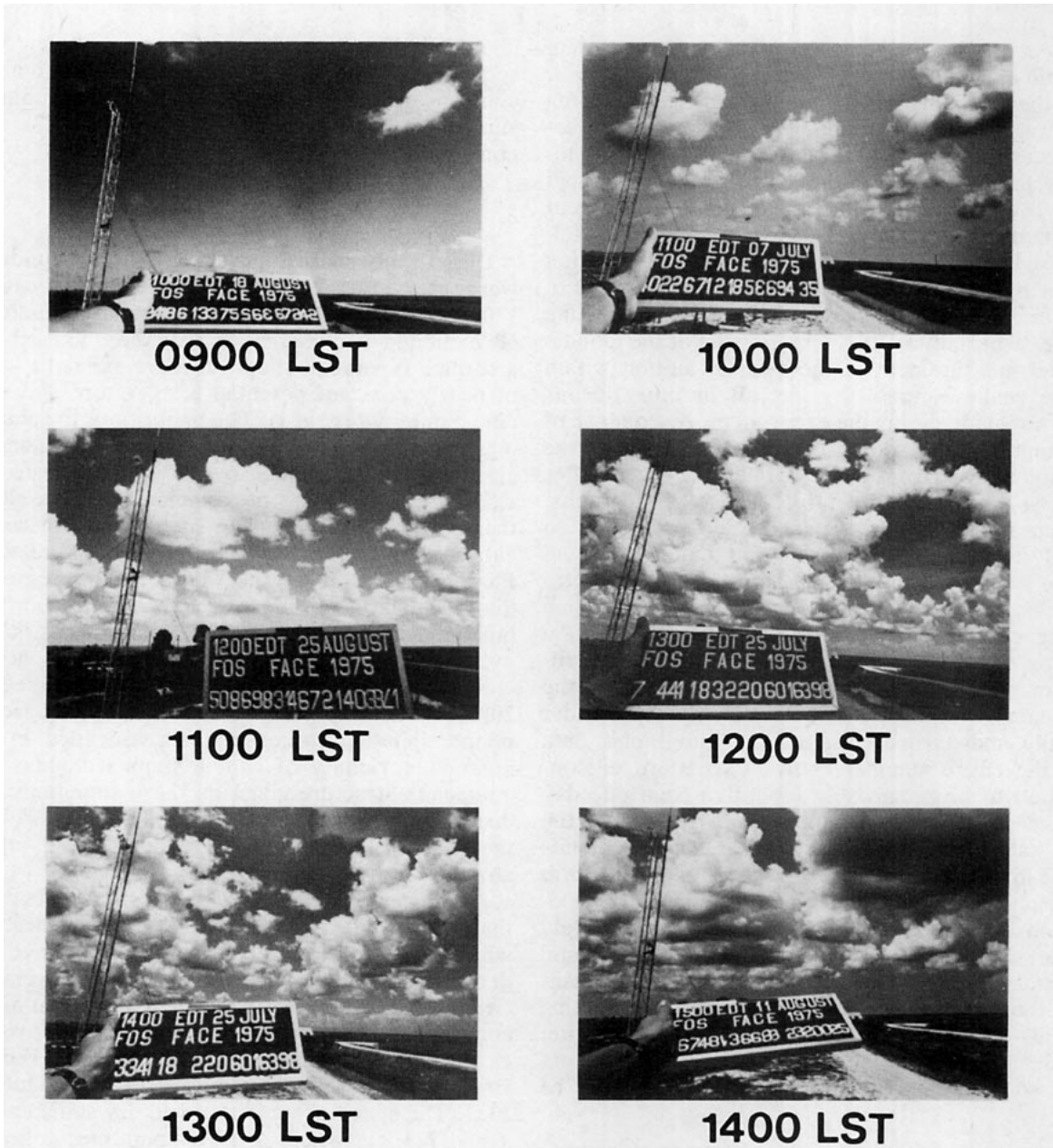

FIG. 1. A sequence of photographs depicting the typical appearance of the cumulus layer from 0900 to 1400 LST under locally undisturbed conditions. Each photograph was taken at the rawinsonde site facing toward the north.

determined from the relative humidity traces, are systematically overestimated by 70–90 m (~7–9 mb). However, the emphasis in this study will be on the mixed-layer and cumulus-layer structures and growth and, therefore, neglect of the above systematic errors will not have a significant effect on the results. Wind data obtained during the experiment will not be considered in this study except to assist in the determination and elimination from the subsequent analysis those cases in which the sounding site was influenced by lake breeze effects from Lake Okeechobee to the north.

Of particular importance to this investigation is a comprehensive sequence of photographs of sky conditions taken during the experiment at the sounding site. Still-camera pictures at 30 min intervals were used as an aid in confirming the existence of a cumulus layer in each instance as well as determining the degree of convective activity at rawinsonde release time.

Both still and time-lapse photography obtained during the experiment reveal a consistent variation in the convective activity over the south Florida peninsula from midmorning until early afternoon

(except on disturbed days). Typically, the first small cumuli appear about 0900 and are widely scattered. As the cumulus layer deepens the cloud area coverage increases somewhat. Time-lapse sequences suggest that the shallow cumuli are initially predominantly updrafts with relatively rapid growth to various levels, not exceeding an apparent common maximum level at a particular time, followed by fairly rapid evaporation and dissipation of each convective element. Weak downward motion is frequently evident during the dissipating stage, especially in the upper portion of the clouds. Direct measurement of the vertical motion within these shallow cumuli by aircraft or other means was not made during the experiment. A sequence of photographs illustrating the time evolution of the cumulus layer from 0900 to 1400 (3.2–8.2 h after sunrise) is shown in Fig. 1. These photographs, except for the first in the sequence, were taken on days in which both mixed and cumulus layers were evident from the sounding data. A photographic sequence for a single day that had sounding evidence for the existence of both layers through the entire day was not available. Although on different dates, the photographs in Fig. 1 show the typical growth behavior of the cumulus layer under locally undisturbed conditions. Photographic data for the entire summer show this pattern of convection to be remarkably repetitive from one day to the next. As the cumulus layer deepens in the early afternoon, groups or lines of cumulus clouds typically develop sufficient vertical extent to form precipitation somewhere over the peninsula. The locations of these precipitating regions are largely determined by the synoptic-scale wind field and coastal geography (Pielke, 1974). This study focuses on those situations in which the precipitating clouds are rather distant from the sounding site. Under these conditions local mean subsidence exists so that mixed and cumulus layers may be identified. This subsidence may be a direct consequence of the sea breeze circulation, due to compensating downward motion in the environment surrounding deep convection (Johnson, 1977), or a combination of both.

TABLE 1. Number of soundings in each category of subcloud layer structure.

	Time (LST)			
	1000	1300	1600	Total
Subcloud layer structure				
Well mixed				
Into clear air*	18	20	9	47
Into cloud base	6	7	2	15
Near cumulonimbi	0	5	1	6
Not well mixed				
Downdraft influenced	0	10	23	33
Others	19	7	2	28
Totals	43	49	37	129
Mixed and cumulus layers evident	7	12	5	24

* Ascent within field of nonprecipitating cumuli.

3. Observed structure

During July and August 1975 three soundings were released on most days at approximately 1000, 1300 and 1600 LST. Out of 129 total soundings, 68 exhibited a mixed-layer structure, i.e., above a surface superadiabatic layer there existed a layer of nearly constant potential temperature and specific humidity (Table 1). The majority of the soundings in this group (47) ascended within a field of nonprecipitating shallow cumuli, but did not penetrate any clouds. In these cases no cumulonimbi were closer than 15 km to the sounding site: in most instances either no cumulonimbi were present over the south Florida peninsula or any that were present were greater than 50 km distant. The cloud cover within 15 km was predominantly cumulus humilis or mediocris with an average area coverage <20%. There were no incidences when stratiform cloud cover exceeded 20%. Fifteen balloons ascended through the bases of nonprecipitating clouds and six ascended in the immediate vicinity of cumulonimbus clouds. The composite structure given by these soundings was discussed by Johnson (1977). Sixty-one or 47% of the total soundings did not exhibit a well-mixed structure at all.

As indicated in Table 1, 24 out of the 47 soundings that showed a mixed layer (ascent into clear air within a field of nonprecipitating cumuli) gave evidence of a cumulus layer topped by an inversion. Ground-based photographs were used as an aid in confirming the existence of the cumulus layer in each case. As an example, Fig. 2 shows the vertical structure of the lower atmosphere on 25 July at 1327. The specific humidity q and dry static energy $s = c_pT + gz$, where T is temperature, z geopotential height and c_p specific heat at constant pressure, are plotted as a function of height. A mixed layer extending to 1410 m with nearly constant s and q and a cumulus layer with nearly constant lapse rates of s and q extending to 2583 m are evident in Fig. 2. Note the increase in stability above the cumulus layer. The fifth photograph in the sequence in Fig. 1 at 1300 on 25 July, 27 min before the time of release of the sounding presented in Fig. 2, shows the cumulus structure in the vicinity of the release site. It is not possible to photogrammetrically determine the cumulus layer depth from the picture; however, the depth indicated by the sounding seems consistent with a rough visual determination from the photograph.

Repeating the above analysis on the other 23

soundings for which both cumulus and mixed layers were evident has enabled a composite of these layers to be constructed. For each sounding a vertical coordinate has been defined that scales all positions in the mixed layer relative to the mixed-layer depth and all positions in the cumulus layer relative to the cumulus-layer depth. The soundings were then averaged using this new vertical coordinate. This method preserves the structure of the layers in the compositing analysis. Fig. 3 shows the composite structure of s and q at the average times of 0952, 1248 and 1526. The average heights of the mixed-layer inversion z_i and the cumulus layer inversion z_c at these times are indicated. The subcloud layer is nearly well-mixed above the surface superadiabatic layer, especially in s. The specific humidity at 0952 and 1248 decreases gradually with height in the mixed layer. These results for the mixed layer are similar to those presented based on the larger group of 47 soundings in Johnson (1977). The cumulus layer is slightly conditionally unstable with nearly constant lapse rates of s and q (except, perhaps, for q at 0952 LST) topped by a stable layer above. Although the upper boundary to the cumulus layer exhibits an inversion, it is not nearly as pronounced as the trade wind inversion observed, say, over the central Atlantic (e.g., Augstein *et al.*, 1974).

The mean thermodynamic structure shown in Fig. 3 is based on a limited number of soundings. Although a statistical analysis of the data might suggest including in Fig. 3 standard deviations of s and q at each level, such an analysis would not be meaningful due to the variation in mixed and cumulus layer inversion heights (Fig. 4). In this study the structure of the cumulus layer and its time evolution are emphasized. Accordingly, the lapse rates of virtual static energy in the cumulus layer

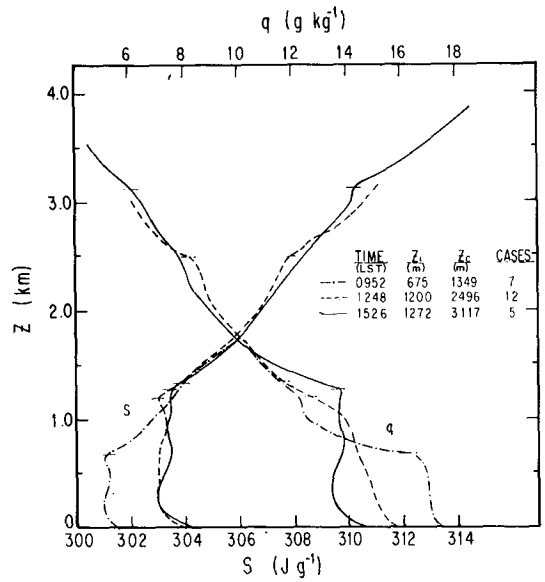

FIG. 3. Composite structure of s and q at the three rawinsonde release times. Horizontal tick marks indicate heights of mixed-layer inversion z_i and cumulus-layer inversion z_c.

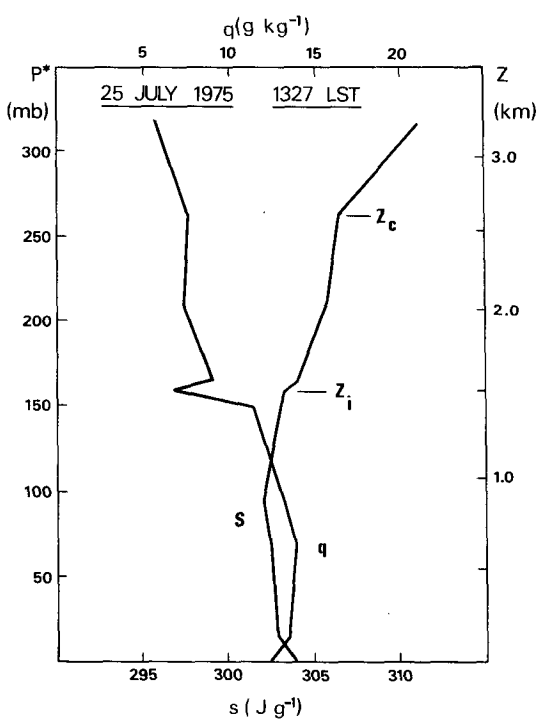

FIG. 2. The mixed-layer and cumulus-layer dry static energy s and specific humidity q at 1327 LST 25 July 1975. P^* refers to the pressure below the surface pressure (1016 mb); z_i and z_c refer to heights of the mixed-layer and cumulus-layer inversions.

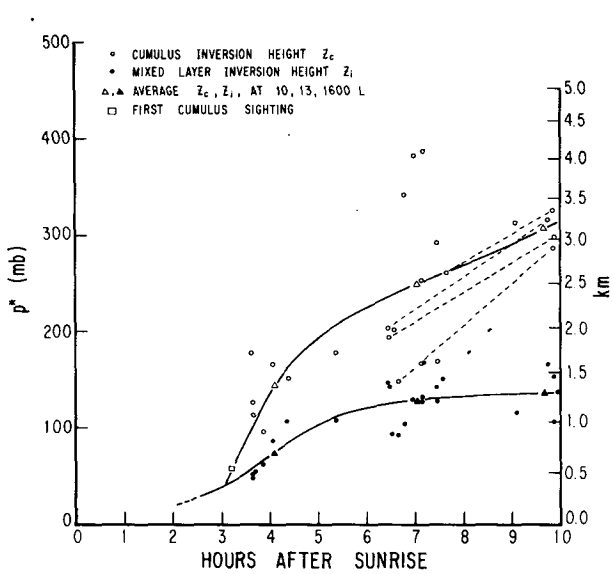

FIG. 4. Mixed-layer and cumulus-layer inversion heights as a function of time after sunrise (0546 LST). P^* is the pressure below the surface pressure (1017 mb). Solid curves have been subjectively determined; dashed lines indicate growth of cumulus layer inversion on four days from 1300 to 1600 LST.

TABLE 2. Lapse rates of virtual static energy in the cumulus layer and the layer above (γ_v,γ_{vt}). Units: J g^{-1} m^{-1}.

	0952 LST	1248 LST	1526 LST
γ_v	$2.9 \pm 1.1 \times 10^{-3}$	$2.9 \pm 1.0 \times 10^{-3}$	$3.0 \pm 0.7 \times 10^{-3}$
γ_{vt}	$4.9 \pm 2.4 \times 10^{-3}$	$5.1 \pm 1.2 \times 10^{-3}$	$4.8 \pm 0.7 \times 10^{-3}$

and the layer above, γ_v and γ_{vt}, and their standard deviations at 0952, 1248 and 1526 have been determined (Table 2). Virtual static energy s_v is defined as $s(1 + 0.61q)$. An interesting result is the nearly constant lapse rate of s_v that exists in each layer throughout the day. Apparently, even though the cumulus layer deepens with time, the stability in and above the cumulus layer remains relatively constant, with values above the cumulus layer 60–75% greater than those within the cumulus layer.

The variation of z_i and z_c with time is shown in Fig. 4. Individual values are indicated clustered about the three central times 1000, 1300 and 1600 LST as well as the averages at these times. Also indicated in this diagram are the average observed time and estimated height of the first small cumuli that were observed in the morning. The average inversion level shortly after sunrise estimated from 1200 GMT (0700 LST) Miami soundings is approximately 150–200 m. Subjectively determined curves have been drawn through the average inversion heights in Fig. 4 even though in the case of the cumulus inversion (z_c) there is significant scatter at 1300. Individual growth rates between 1300 and 1600 that could be determined for four of the five 1600 soundings agree reasonably well with that given by the averages for 1300 and 1600 as shown in Fig. 4. Thus, the use in the subsequent section of the composite representation of the growth of the cumulus layer by the solid curves seems well justified. Johnson (1977) discussed the growth of the mixed layer and effect of peninsula-scale deep cumulus convection and compensating subsidence in reducing the growth rate of z_i several hours before noon. The vertical separation between the two curves in Fig. 4 represents the average depth of the cumulus layer and the time variation for the 24 soundings, although it must be recognized that the time variation on a particular day may be quite different from this average, especially if deep convection occurs locally.

4. Model representation of observed behavior

We assume a mixed layer with a constant virtual dry static energy $s_{vm} = s_m(1 + 0.61\, q_m)$, where s_m, q_m are the mixed layer mean values of s, q, surmounted by a cumulus layer with a constant lapse rate $\gamma_v = d\bar{s}_v/dz$ (Fig. 5). A constant lapse rate γ_{vt} is also assumed above the cumulus layer. This structure, which is consistent with that shown in Fig. 3, is assumed to exist in the region between clouds or the cloud environment. In the following analysis an overbar will be used to denote a horizontal average over a mesoscale area large enough to contain a statistically representative population of cumulus clouds within the nonprecipitating convective field, yet small compared to the area of the Florida peninsula. A tilde will be used to refer to values in the cumulus environment within the mesoscale area defined above. Advective effects and radiative jumps at the tops of the mixed layer z_i and cumulus layer z_c are neglected. The latter assumption should be justified for the small fractional area cloud coverage considered here. The data of Holland and Rasmusson (1973) suggest a radiative jump near the base of the trade inversion of $\sim$0.5 K day^{-1}; however, the moisture discontinuity across the cumulus layer inversion over Florida is considerably smaller than that for the trade inversion. Johnson (1977) showed that advective effects are not important in the growth of the mixed layer at the sounding site.

Following the development and notation of the previous paper by Johnson (1977) it was shown that the equations for the time evolution of the mixed layer inversion height z_i and the inversion strength $\Delta s_v = \bar{s}_v(z_b) - s_{vm}$ are

$$\frac{\partial z_i}{\partial t} = \tilde{w}_i - \frac{(\widetilde{s_v'w'})_i}{\Delta s_v}, \tag{1}$$

$$\frac{\partial \Delta s_v}{\partial t} = -\frac{(\widetilde{s_v'w'})_i}{\Delta s_v}\gamma_v - \frac{1}{\Delta z}[\overline{(s_v'w')}_s - \overline{(s_v'w')}_i] + \int_0^{\lambda(z_b)} \delta_u(\lambda,z_b)[s_{vu}(\lambda,z_b) - \bar{s}_v(z_b)]d\lambda, \tag{2}$$

where it is assumed that cloud-base level z_b corresponds to the top of the transition layer, $\tilde{w}_i$ and $(\widetilde{s_v'w'})_i$ are the vertical velocity and buoyancy flux at z_i in the cloud environment, $\overline{(s_v'w')}_s$ is the buoyancy flux at z_s and

$$\rho\overline{(s_v'w')}_i = M_u(z_i)[s_{vu}(z_i) - s_{vm}] + \int_0^{\lambda(z_i)} m_d(\lambda,z_i)[s_{vd}(\lambda,z_i) - s_{vm}]d\lambda + \rho(\widetilde{s_v'w'})_i,$$

where

λ	entrainment rate
$\delta_u(\lambda,z_b)$	updraft detrainment rate of cloud type λ at z_b
$s_{vu,d}(\lambda,z)$	updraft, downdraft virtual static energy of cloud type λ at z
$s_{vu}(z_i)$	constant for all cloud types
$M_u(z_i)$	total cumulus updraft mass flux at z_i
$m_d(\lambda,z_i)$	downdraft mass flux per unit λ at z_i
Δz	$z_i - z_s$
ρ	air density.

The nonprecipitating cloud field has been represented by a spectrum of cloud sizes (after Arakawa

and Schubert, 1974) ranging from several meters to 1–2 km depth given in terms of fractional mass entrainment rates λ. Each cloud is assumed to have an updraft and downdraft that both entrain the same environmental air and both contribute to the flux at z_i. In (2) the effects of detrainment from the sides of downdrafts at z_b, although neglected, could be included by adding a term analogous to the updraft detrainment term. In the above it has been assumed that the fractional area occupied by clouds is small to permit the approximation $\bar{s}_v \approx \bar{s}_v$. The set (1), (2) is similar to that proposed by Betts (1976), although he uses a single cloud mass flux model.

The model is next extended to the cumulus layer where a constant lapse rate γ_v is assumed in accordance with observation (Figs. 3 and 5). The heat budget at the cumulus inversion yields (as in Mak, 1976)

$$\frac{\partial z_c}{\partial t} = \bar{w}_c + \frac{1}{\Delta s_{vt}}[Le_t \Delta z_{ct} - \overline{(s_v'w')}_c], \qquad (3)$$

where subscript c refers to values at the base of the cumulus inversion,

$$e_t \equiv \frac{1}{\Delta z_{ct}} \int_{z_c}^{z_t} (\bar{e} - \bar{c}) dz$$

where z_t is the cumulus inversion top and $\bar{e}$, $\bar{c}$ are evaporation, condensation rates and

$$\Delta z_{ct} = z_t - z_c,$$

$$\Delta s_{vt} = \bar{s}_v(z_t) - \bar{s}_v(z_c),$$

$$\overline{(s_v'w')}_c = \frac{1}{\rho} \int_0^{\lambda(z_c)} m_u(\lambda, z_c) \times [s_{vu}(\lambda, z_c) - \bar{s}_v(z_c)] d\lambda + \widetilde{(s_v'w')}_c.$$

Figuring in the heat budget at z_c are the net evaporation e_t in the cumulus inversion and the total buoyancy flux $\overline{(s_v'w')}_c$, at z_c, which has contributions from both cumulus updrafts (downdrafts are neglected at z_c) and transports in the near-cloud environment. It is assumed that the cumulus towers overshoot z_c, leading to the downward flux of potentially warmer air from above in the immediate vicinity of the cloud. Additionally, a uniform subsidence $\bar{w}_c$ occurs in the between-cloud region such that the mean mass flux is given by

$$\rho \bar{w}_c = M_u(z_c) + \rho \bar{w}_c. \qquad (4)$$

Assuming horizontal homogeneity of the averaged variables, the equation for $\bar{s}_v$ in the cumulus layer is to a good approximation

$$\frac{\partial \bar{s}_v}{\partial t} + \bar{w}\gamma_v = -\frac{\partial}{\partial z}\overline{(s_v'w')} + \bar{Q}_R + L(\bar{c} - \bar{e}), \qquad (5)$$

where Q_R is the radiative heating rate. Integrating (5) from cloud-base z_b to the top of the cumulus layer z_c, we obtain after some manipulation

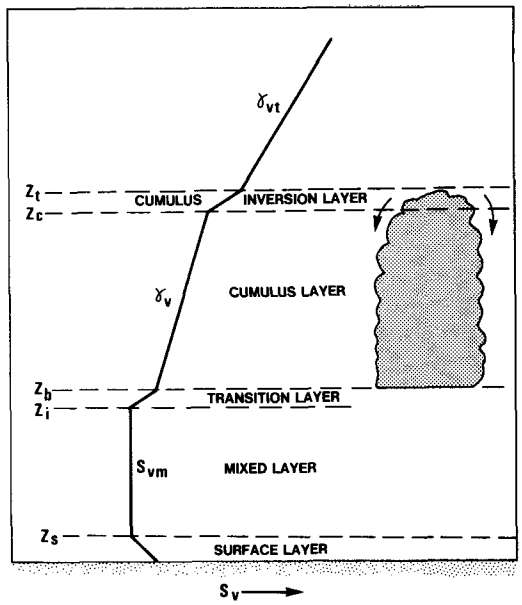

FIG. 5. Schematic illustration of mixed-layer and cumulus-layer structure.

$$\frac{\partial \bar{s}_v(z_c)}{\partial t} + \gamma_v\left(\langle \bar{w} \rangle - \frac{\partial z_c}{\partial t}\right) = \frac{1}{\Delta z_c}[\overline{(s_v'w')}_b - \overline{(s_v'w')}_c] + \langle \bar{Q}_R \rangle + L\langle \bar{c} - \bar{e} \rangle, \qquad (6)$$

where

$$\langle\ \rangle \equiv \frac{1}{\Delta z_c}\int_{z_b}^{z_c} (\ )dz, \quad \Delta z_c = z_c - z_b,$$

$$\overline{\rho(s_v'w')}_b = M_u(z_b)[s_{vu}(z_b) - \bar{s}_v(z_b)] + \int_0^{\lambda(z_b)} m_d(\lambda, z_b)[s_{vd}(\lambda, z_b) - \bar{s}_v(z_b)]d\lambda.$$

In the above it is assumed that $s_{vu}(z_b)$ is the same for all cloud types. At and above z_t cumulus activity ceases to exist and we have

$$\frac{\partial \bar{s}_v(z_t)}{\partial t} + \bar{w}_t\gamma_{vt} = \gamma_{vt}\frac{dz_c}{dt} + \bar{Q}_{Rt}, \qquad (7)$$

where the subscript t refers to values at z_t and $dz_c/dt \approx dz_t/dt$. Since the cumulus inversion is relatively thin, $\bar{w}_t \approx \bar{w}_c$, and assuming $\bar{Q}_{Rt} \approx \langle \bar{Q}_R \rangle$ as it should for a widely scattered cloud field (<20% cloud coverage), then (6) can be subtracted from (7) and combined with (3) to give

$$\frac{\partial \Delta s_{vt}}{\partial t} = \frac{1}{\Delta s_{vt}}[Le_t \Delta z_{ct} - \overline{(s_v'w')}_c] \times (\gamma_{vt} - \gamma_v) + \gamma_v(\langle \bar{w} \rangle - \bar{w}_c) + \frac{1}{\Delta z_c} \times [\overline{(s_v'w')}_c - \overline{(s_v'w')}_b] - L\langle \bar{c} - \bar{e} \rangle. \qquad (8)$$

The term $L\langle\bar{c} - \bar{e}\rangle$ represents the net condensation in the nonprecipitating cumulus layer. It is positive since condensation exceeds evaporation in the cumulus layer as cloud droplets are transported into the cumulus inversion layer where evaporation exceeds condensation. This term also increases with time as the cloud volume increases.

If the second and fourth terms on the right-hand side of (8) are neglected, as will be shown in the next section is justified for the Florida data, then we see that Eq. (8) for the strength of the cumulus inversion Δs_{vt} is similar in form to (2) for the mixed layer inversion strength Δs_v. Missing from (8), however, is a detrainment term as a result of the fact that detrainment in the case of the cumulus inversion occurs within the inversion, whereas in the case of the transition layer detrainment occurs at a boundary, the level of cloud base.

The set (1), (2), (3) and (8) is a system of coupled equations for the four unknowns z_i, z_c, Δs_v, Δs_{vt}. Certain closure assumptions are required, however, before solution is possible. In the same manner as Johnson (1977), the standard closure condition (Tennekes, 1973) for the mixed layer $(\widetilde{s_v'w'})_i = -k(\overline{s_v'w'})_s$, where k = constant, is used. An additional closure condition for $(\widetilde{s_v'w'})_c$ is required to solve this problem. Sarachik (1974, unpublished manuscript) proposed that $(\widetilde{s_v'w'})_c$ might be related to the surface latent heat flux or evaporation. Although it would be advantageous to relate $(\widetilde{s_v'w'})_c$ to a known buoyancy flux at some other level as is done for the mixed layer, such a relationship is difficult to determine because of the intermittent and complex nature of the moist convection within the cumulus layer. However, it would seem reasonable that $(\widetilde{s_v'w'})_c$ might be directly proportional to the buoyancy flux in all cumulus updrafts at z_c, i.e.,

$$(\widetilde{s_v'w'})_c = -\kappa \int_0^{\lambda(z_c)} m_u(\lambda,z_c)[s_{vu}(\lambda,z_c) - \bar{s}_v(z_c)]d\lambda,$$

where κ is a constant. This quantity should provide a measure of the magnitude of the updraft overshooting above z_c and, hence, downward entrainment of potentially warmer air from above. An obvious shortcoming of the proposed closure condition is that it does not include the effects of the cumulus inversion strength Δs_{vt} or stability above the inversion γ_{vt}. It is noted, however, that the use of a constant k in the closure for the mixed layer has met with considerable success. Unfortunately, the experimental data do not provide sufficient information to determine $\bar{w}(z)$ and, thus, $m_u(\lambda,z)$, $m_d(\lambda,z)$ and $\delta_u(\lambda,z)$; so the above hypothesis could not be tested. The following section describes the results that were obtainable from a limited application of the model to the 1975 FACE data.

5. Limited application to FACE data

The model has been applied using the observed composite growth rates of the mixed and cumulus layers shown in Fig. 4. Rather than solve (1)–(3) and (8) for z_i, z_c, Δs_v and Δs_{vt}, the observed time dependence of z_i, z_c is used to solve for Δs_v, Δs_{vt}, $\bar{w}_i$ and $(\overline{s_v'w'})_c$. Since the cumulus buoyancy flux at z_c is upward (positive) and $(\widetilde{s_v'w'})_c$ is downward (negative), the magnitude of $(\overline{s_v'w'})_c$ obtained in this manner will represent a lower bound to $|(\widetilde{s_v'w'})_c|$. Without knowing $\bar{w}(z)$ and, hence, the heating and moistening effects of the cumulus convection (Q_1, Q_2 as in Yanai *et al.*, 1973), it is not possible to separate the cumulus and environmental flux components to the total buoyancy flux at z_c. Therefore, the results of this section are limited in the sense that only a lower bound to $|(\widetilde{s_v'w'})_c|$ can be determined.

A number of approximations are necessary to complete the solution. Since the difference between $\langle\bar{w}\rangle$ and $\bar{w}_c$ is likely $\lesssim 1$ cm s^{-1} for the shallow convective field under study, the term $\gamma_v(\langle\bar{w}\rangle - \bar{w}_c)$ in (8) is $\lesssim 10\%$ of the largest terms in the equation and is neglected. Using the estimate $L\langle\bar{c} - \bar{e}\rangle \approx 3$ K day^{-1} suggested by the results of Nitta (1975) for the trade inversion we see that the last term in (8) can similarly be neglected. The evaporation rate e_t is approximated by $q_l \Delta M_u/\Delta z_{ct}$, where $\Delta M_u/\Delta z_{ct}$ represents the detrainment rate in the cumulus inversion of depth Δz_{ct}, ΔM_u being the jump of the cumulus mass flux to zero at the top of the inversion layer and q_l the cloud-top liquid water mixing ratio. For the scattered shallow convection present here terms in (2) and (8) containing $M_u(s_{vu} - \bar{s}_v)$ are small compared to $(\overline{s_v'w'})_s$ and $(\overline{s_v'w'})_c$ for reasonable estimates of cloud-environment differences in s_v and cumulus mass fluxes (Johnson, 1977). As a first approximation the detrainment term in (2) and downdraft terms in (2) and (8) are neglected, although measurements are not available to justify this step.

Results of the numerical solution of (1)–(3) and (8) are shown in Table 3. The integration begins at sunrise ($t = 0$) with initial values of Δs_v and $\bar{w}_i$ of 3 K and 0, respectively. As pointed out in Johnson (1977), results are insensitive to the choices, within reasonable bounds, of initial conditions. In these computations we have assumed ΔM_u is a specified fraction α of $M_u(z_b)$ and set $q_l = 0.001$ since direct measurements of cloud-top liquid water contents were not made. Results are not particularly sensitive to q_l since the evaporation term in (3) is of secondary importance as pointed out later. We approximate $M_u(z_b)$ in e_t by $-\rho\bar{w}_i$ [equivalent to the statement that $M_u(z_b)$ is considerably larger than $|\bar{w}_i|$] and set $\bar{w}_c = \beta\bar{w}_i$, where β is a constant. The parameters α and β have been introduced simply because $\bar{w}(z)$ is not known: α is essentially a measure

TABLE 3. Computed inversion strengths (Δs_v, Δs_{vt}), buoyancy flux $(\overline{s_v'w'})_c$ and environmental subsidence ($\bar{w}_i$). $\alpha = \Delta M_u/M_u(z_b)$; $\beta = \bar{w}_c/\bar{w}_i$; $k = 0.2$.

Time after sunrise (h)	α	β	$\frac{\bar{w}_c}{\bar{w}_i}$	Δs_v	Δs_{vt}	$(\overline{s_v'w'})_c$	$(\overline{s_v'w'})_s$	$\bar{w}_i$
$t = 3$				1.8	0.1	0	16	0
$t = 6$	1	1	2.0	0.8	2.4	−21	25	−8.0
	0.5	1	1.5	0.8	2.2	−27	25	−8.0
	0.1	1	1.1	0.8	2.1	−32	25	−8.0
	0.2	2	2.2	0.8	2.3	−51	25	−8.0
$t = 9$	1	1	2.0	1.1	4.0	−36	22	−8.5
	0.5	1	1.5	1.1	3.6	−41	22	−8.5
	0.1	1	1.1	1.1	3.3	−44	22	−8.5
	0.2	2	2.2	1.1	3.8	−80	22	−8.5

Units: Δs_v(K); $\overline{s_v'w'}$ (cm K s^{-1}); $\bar{w}_i$(cm s^{-1}).

of evaporation in the cumulus inversion—larger values imply more evaporation; β is a measure of the magnitude of the mean subsidence $\bar{w}_c$, which must be specified in (3) and (8), in relation to $\bar{w}_i$. The quantity $\alpha + \beta$ is $\bar{w}_c/\bar{w}_i$ or the ratio of the environmental subsidence at z_c and z_i. The sensitivity of the model to α and β is shown in Table 3. At $t = 3$ h the cumulus layer begins to grow (Fig. 4) and at this time we set initial values of Δs_{vt} and $(\overline{s_v'w'})_c$ equal to 0.1 K and 0, respectively. Values of the surface buoyancy flux $(\overline{s_v'w'})_s$ determined as in Johnson (1977) are shown for comparison.

An important result from Table 3 is the significant increase with time of $|(\overline{s_v'w'})_c|$, and hence $|(\widetilde{s_v'w'})_c|$, from $t = 3$ to $t = 9$ h. Also note that $|(\widetilde{s_v'w'})_c|$ exceeds $(\overline{s_v'w'})_s$ by a large amount at $t = 9$ h. As mentioned earlier, it is not possible with the data given to partition $(\overline{s_v'w'})_c$ into its moist convective and $(\widetilde{s_v'w'})_c$ components, a factor which limits the interpretation of these results. Since there is a significant increase in $|(\overline{s_v'w'})_c|$ when β is increased from 1 to 2 it is obvious that any future experiment designed to determine the components of the buoyancy flux at the top of the cumulus layer will require an accurate determination of $\bar{w}(z)$. The large increase in $|(\overline{s_v'w'})_c|$ when β is increased from 1 to 2 reflects an increased downward heat flux into the cumulus layer that is necessary when $\bar{w}_c$ is increased so that (3) is satisfied using the observed $\partial z_c/\partial t$. The evaporation term is of secondary importance as indicated by the sensitivity of the results to variations in α, although its effect cannot be neglected.

6. Summary and conclusions

This study reports on 1975 Florida Area Cumulus Experiment (FACE) findings concerning the structure of the planetary boundary layer over south central Florida under locally undisturbed conditions. From a series of rawinsonde observations (129 total) during July and August at approximately 1000, 1300 and 1600 LST, 24 have been identified as presenting both mixed and cumulus layer structures. These soundings have been composited to provide a representation of the average structure of the two layers. The inversion that exists at the top of the cumulus layer is much less pronounced than the trade wind inversion as might be expected considering the relatively rapid growth and short lifetime of this phenomenon. The observed time evolution of the mixed-layer and cumulus-layer inversion heights is shown for the group of 24 soundings. Each sounding in this group ascended through a field of shallow nonprecipitating cumuli (no cloud penetration, however). The first cumuli of the day appear approximately 3 h after sunrise and under locally undisturbed conditions, situations where deep cumulonimbus clouds are located over the peninsula rather distant (>15 km) from the sounding site, significant mesoscale subsidence approaching 10 cm s^{-1} at the top of the mixed layer is observed to restrict the growth of the mixed and cumulus layers.

A model for the growth of the mixed and cumulus layers is presented that includes effects of updraft mass flux, detrainment and evaporation. A closure assumption is proposed that relates the buoyancy flux in the cloud environment at the base of the cumulus inversion to the buoyancy flux within cumulus updrafts at that level. Due to the unavailability of data providing an estimate of the local mean subsidence velocity $\bar{w}$, however, this hypothesis could not be tested. Application of the model to the 1975 FACE data has provided lower bound estimates to the downward buoyancy flux at the cumulus inversion. The results of this study point to the need for accurate determination of $\bar{w}$ if models for the growth of the mixed and cumulus layers are to be tested against observations. The south Florida peninsula appears to be an excellent location for more detailed studies of the dynamics

of the mixed and cumulus layers including the more complicated effects of moist convective downdrafts.

Acknowledgments. My appreciation is extended to Jack Thomas for providing the rawinsonde data used in this study. I thank Ron Holle for supplying photographic data and others at the National Hurricane and Experimental Meteorology Laboratory, Coral Gables, Florida, involved in completion of the 1975 Florida Area Cumulus Experiment. Thanks also go to Cindy Ruka for her excellent typing of the manuscript.

REFERENCES

Albrecht, B. A., 1977: A time-dependent model of the trade wind boundary layer. Ph.D. thesis, Colorado State University, Fort Collins, 174 pp.

Arakawa, A., and W. Schubert, 1974: Interaction of cumulus cloud ensemble with the large-scale environment, Part 1. *J. Atmos. Sci.*, **31**, 674–701.

Augstein, A., H. Schmidt and F. Ostapoff, 1974: The vertical structure of the atmospheric boundary layer in undisturbed trade winds over the Atlantic Ocean. *Bound.-Layer Meteor.*, **6**, 129–150.

Betts, A. K., 1973: Non-precipitating cumulus convection and its parameterization. *Quart. J. Roy. Meteor. Soc.*, **99**, 178–196.

——, 1976: Modeling subcloud layer structure and interaction with a shallow cumulus layer. *J. Atmos. Sci.*, **33**, 2363–2382.

Bunker, A. F., B. Haurwitz, J. S. Malkus and H. Stommel, 1949: Vertical distribution of temperature and humidity over the Caribbean Sea. *Pap. Phys. Oceanogr. Meteor.*, No. 11, 1–82.

Carson, D. J., 1973: The development of a dry inversion-capped convectively unstable boundary layer. *Quart. J. Roy Meteor. Soc.*, **99**, 450–467.

Ficker, H., 1936: Die Passatinversion. *Veroeffentl. Meteorol. Inst. Univ. Berlin*, **1**, No. 4.

Garstang, M., and A. K. Betts, 1974: A review of the tropical boundary layer and cumulus convection: Structure, parameterization and modeling. *Bull. Amer. Meteor. Soc.*, **55**, 1195–1205.

Holland, J. Z., and E. M. Rasmusson, 1973: Measurements of the atmospheric mass, energy and momentum budgets over a 500-kilometer square of tropical ocean. *Mon. Wea. Rev.*, **101**, 44–55.

Johnson, R. H., 1977: Effects of cumulus convection on the structure and growth of the mixed layer over south Florida. *Mon. Wea. Rev.*, **105**, 713–724.

Lilly, D. K., 1968: Models of cloud-topped mixed layers under a strong inversion. *Quart. J. Roy. Meteor. Soc.*, **94**, 292–309.

Mak, M. K., 1976: A model study of the downstream variation of the lower tradewind circulation. *Tellus*, **28**, 97–107.

Malkus, J. S., 1958: On the structure of the trade wind moist layer. *Pap. Phys. Oceanogr. Meteor.*, No. 13, 1–48.

Nitta, T., 1975: Observational determination of cloud mass flux distributions. *J. Atmos. Sci.*, **32**, 73–91.

Ogura, Y., 1977: A note on the downstream variation of the lower trade-wind circulation. *Tellus*, **29**, 240–244.

——, J. Russell and H.-R. Cho, 1977: A semi-empirical model of the trade-wind inversion. *J. Meteor. Soc. Japan*, **55**, 209–221.

Pielke, R., 1974: A three-dimensional numerical model of the sea breezes over south Florida. *Mon. Wea. Rev.*, **102**, 115–139.

Riehl, H., C. Yeh, J. S. Malkus and N. E. LaSeur, 1951: The north-east trade of the Pacific Ocean. *Quart. J. Roy. Meteor. Soc.*, **77**, 598–626.

Sarachik, E. S., 1974: A simple theory for the vertical structure of the tropical atmosphere. Harvard University Rep., 19 pp.

Simpson, J., and W. L. Woodley, 1975: Florida area cumulus experiments: 1970–73 rainfall results. *J. Appl. Meteor.*, **14**, 734–744.

Tennekes, H., 1973: A model for the dynamics of the inversion above a convective boundary layer. *J. Atmos. Sci.*, **30**, 558–567.

Yanai, M., S. Esbensen and J. H. Chu, 1973: Determination of bulk properties of tropical cloud clusters from large-scale heat and moisture budgets. *J. Atmos. Sci.*, **30**, 611–627.